2010

Kinetics of Hedgehog-Dependent Full-Length Gli3 Accumulation in Primary Cilia and Subsequent Degradation

Xiaohui Wen

Cary Lai
University of San Francisco, cklai2@usfca.edu

Marie Evangelista

Jo-Anne Hongo

Frederic J. de Sauvage

See next page for additional authors

Authors

Xiaohui Wen, Cary Lai, Marie Evangelista, Jo-Anne Hongo, Frederic J. de Sauvage, and Suzie J. Scales

Kinetics of Hedgehog-Dependent Full-Length Gli3 Accumulation in Primary Cilia and Subsequent Degradation[∇][†][‡]

Xiaohui Wen,[1] Cary K. Lai,[1] Marie Evangelista,[1] Jo-Anne Hongo,[2]
Frederic J. de Sauvage,[1] and Suzie J. Scales[1]*

Departments of Molecular Biology[1] and Antibody Engineering,[2] Genentech, Inc., 1 DNA Way, South San Francisco, California 94080

Hedgehog (Hh) signaling in vertebrates depends on intraflagellar transport (IFT) within primary cilia. The Hh receptor Patched is found in cilia in the absence of Hh and is replaced by the signal transducer Smoothened within an hour of Hh stimulation. By generating antibodies capable of detecting endogenous pathway transcription factors Gli2 and Gli3, we monitored their kinetics of accumulation in cilia upon Hh stimulation. Localization occurs within minutes of Hh addition, making it the fastest reported readout of pathway activity, which permits more precise temporal and spatial localization of Hh signaling events. We show that the species of Gli3 that accumulates at cilium tips is full-length and likely not protein kinase A phosphorylated. We also confirmed that phosphorylation and βTrCP/Cul1 are required for endogenous Gli3 processing and that this is inhibited by Hh. Surprisingly, however, Hh-dependent inhibition of processing does not lead to accumulation of full-length Gli3, but instead renders it labile, leading to its proteasomal degradation via the SPOP/Cul3 complex. In fact, full-length Gli3 disappears with faster kinetics than the Gli3 repressor, the latter not requiring SPOP/Cul3 or βTrCP/Cul1. This may contribute to the increased Gli3 activator/repressor ratios found in IFT mutants.

The Hedgehog (Hh) signaling pathway is important for establishment of left-right asymmetry and formation of various organs during vertebrate embryonic development (30, 44, 49, 86), but it is mainly quiescent in adults. Inappropriate reactivation, however, contributes to various cancers, thus providing an impetus for further research (for recent reviews, see references 33 and 73).

In vertebrates, the Hh signal transduction cascade is initiated by the Hh ligand binding to its receptor Patched 1 (Ptch), which abolishes Ptch's repression of Smoothened (Smo), enabling this seven-transmembrane G-protein-coupled receptor-like protein to transduce the Hh signal via a complex of cytoplasmic proteins (53, 62). This culminates in activation of a set of transcription factors termed Gli1, Gli2, and Gli3 (69) which modulate Hh pathway target gene transcription in the nucleus (34, 68). Unlike in *Drosophila melanogaster*, where the single Gli homolog Cubitus interruptus (Ci) functions as a transcriptional activator when intact (CiFL) and as a repressor (CiR) when cleaved (2, 4), Gli1 is thought not to be processed and to function solely as a transcriptional activator to enhance signaling (3, 15), being upregulated by pathway activity (45). By contrast, Gli2 and Gli3 can be processed, acting as activators when intact and as N-terminal repressors when cleaved (15, 41, 72, 76, 87).

Gli2 and Gli3 processing is phosphorylation and proteasome dependent: in the absence of Hh, they are phosphorylated at

four to six sites by protein kinase A (PKA), which primes them for further phosphorylation by glycogen synthase kinase 3β (GSK3β) and casein kinase 1 (CK1) (56, 81, 87, 88). The phosphorylated residues provide a high-affinity binding site for βTrCP, which in turn recruits the SCF (Skp1/Cullin1/F-box) ubiquitin ligase complex to target full-length, ~190-kDa Gli3 (Gli3FL) and ~185-kDa Gli2 (Gli2FL) for cleavage via the ubiquitin-proteasome pathway (81, 88) to generate the ~83-kDa Gli3 (Gli3R) and ~78-kDa Gli2 (Gli2R) N-terminal repressors, respectively, while the C termini are assumed to be completely degraded (57). Hh stimulation represses this processing and is thought to result in a predominance of full-length (presumably activator) forms of Gli2A and Gli3A. Regulation of Gli3 processing is especially important in limb development, with the appropriate ratio of Gli3FL and Gli3R being essential for proper digit number and identity (42, 82) and a diminishing gradient of Gli3R resulting in derepression of Hh target genes from the anterior to the posterior of the limb bud (26).

The paradigm of vertebrate Hh signaling has shifted considerably with the seminal discovery that components of primary cilia exert crucial roles during mouse tissue patterning and development (29), which has been expertly reviewed in references 16, 66, and 94. The eukaryotic primary cilium is a microtubule-based membrane protrusion that is assembled and maintained by the bidirectional intraflagellar transport (IFT) machinery (39). Mutations in IFT subunits *Ift88*, *Ift172*, and *Ift122* and motors *Kif3a* and *Dync2h1* all result in polydactyly due to impaired Gli3 processing (14, 25, 28, 29, 43, 47). Moreover, all three Glis and their binding partner Suppressor of Fused (SuFu) have been found in primary cilia (25), while Ptch is only there under unstimulated conditions, with Smo replacing it upon Hh stimulation (13, 65).

Although Gli2 and Gli3 localize to the tips of primary cilia

* Corresponding author. Mailing address: Genentech, 1 DNA Way, MS37, South San Francisco, CA 94080. Phone: (650) 225-1510. Fax: (650) 225-6412. E-mail: sscales@gene.com.

(25, 36) in an Hh-dependent manner in some cell lines (18), it is not well understood how quickly this happens or what modifications occur in the cilia. By generating antibodies recognizing endogenous Gli2 and Gli3, we show here that full-length Gli2 and Gli3 accumulate at cilium tips within 5 min of Hh stimulation. This rapid Hh response is useful for investigation of ciliary events in the Hh pathway, permitting us to discover, for example, that PKA stimulation with forskolin (FSK) inhibits Gli3 accumulation. Furthermore, by Western blotting, we unexpectedly found that while Hh signaling does inhibit endogenous Gli3 processing, this does not result in accumulation of the full-length Gli3 precursor, instead promoting its degradation via SPOP, Cul3, and the proteasome, analogous to the degradation of CiA by Hh-induced MATH and BTB domain-containing protein (HIB) and Cullin3 (Cul3) in *Drosophila* (32, 35, 55, 97). Moreover, we confirmed that IFT is required for efficient Gli3 processing and found it is also required for degradation of Gli3FL.

MATERIALS AND METHODS

Cell culture. COS7, IMCD3 (murine intermedullary collecting duct), NIH 3T3 fibroblast, and S12 (*Gli*-luciferase stably transfected C3H10T1/2 osteoblast [21]) cells were maintained in high-glucose Dulbecco's modified Eagle's medium supplemented with 10% fetal bovine serum (FBS), 10 mM HEPES, and 2 mM L-glutamine. S12 and 3T3 cells were never allowed to become >70% confluent, to maintain proper ciliation and Hh signaling. Mouse embryonic fibroblasts (MEFs) were isolated from embryonic day 10.5 (E10.5) embryos following standard procedures and maintained in the above medium plus 100 μM β-mercaptoethanol (Calbiochem, La Jolla, CA), 100 μM nonessential amino acids, 1 mM sodium pyruvate, and 50 μg/ml penicillin-streptomycin (all from Gibco, Grand Island, NY). Hh stimulation was carried out by serum starving cells in appropriate growth medium with only 0.5% FBS for 16 to 24 h and adding 200 ng/ml octyl-Shh (80) (four times higher than that needed to saturate *Gli*-luciferase activity in S12 cells) concurrently or after appropriate intervals for time course analyses.

Antigen production. N- and C-terminal fragments of human Gli1 (amino acids [aa] 2 to 151 and aa 958 to 1106 of NM_005269); Gli2 (aa 2 to 199 and aa 827 to 1126 of NM_030380, the nonsense-mediated mRNA decay sequence lacking the 324-aa autoinhibitory N-terminal domain [72], which corresponds to aa 330 to 544 [Gli2N] and 1172 to 1471 [Gli2C] of the NM_005270 full-length Gli2 sequence); and Gli3 (conserved aa 2 to 184 and aa 1365 to 1547 of the 1,596-aa M34366 Gli3 variant [70], selected as the most C-terminal region conserved in both reported C-terminal frameshift variants [1,596 and 1,580 aa] of human and mouse Gli3); and the mouse Smo C-terminal tail (aa 550 to 793 of P56726) were subcloned into the in-house pSt239 expression vector with N-terminal unizyme His (HQ) tags. Antigens were expressed in 58F3 *Escherichia coli* and purified over a Ni-nitrilotriacetic acid (NTA) column (Qiagen, Valencia, CA) followed by gel filtration on a Superdex 200 column in 20 mM 2′-(morpholino)ethanesulfonic acid (MES; pH 6.0), 6 M GdnHCl as previously described (37). Pooled purified antigen fractions were reduced with 50 mM dithiothreitol (DTT), acidified with 2.5% (vol/vol) acetic acid, dialyzed against 1 mM HCl, and then flash-frozen in the presence of 4% (wt/vol) mannitol. Gli C termini were purified over a Ni-NTA column under native conditions in the presence of 5 mM β-mercaptoethanol, followed by anion exchange and size exclusion chromatography in phosphate-buffered saline (PBS) containing 250 mM NaCl and 5 mM DTT. Antigens were stored at −80°C until use.

Generation of anti-Gli rabbit pAbs. To maximize the chances of obtaining functional antibodies for immunofluorescence (IF), half of each Gli antigen preparation was fixed for 20 min at room temperature in 3% paraformaldehyde (PFA; Electron Microscopy Sciences, Hatfield, PA), quenched with 50 mM NH4Cl (Sigma, St. Louis, MO) for 10 min at room temperature, and then dialyzed against PBS. The five fixed HQ-Gli N- and C-terminal antigens (Gli2C did not yield sufficient material for immunization in rabbits) were mixed 1:1 with their unfixed counterparts, and 500 μg was used to immunize two New Zealand White rabbits (labeled A and B), each using a 1:1 mixture of antigen and complete Freund's adjuvant, followed by 500-μg boosts every other week with a 1:1 mixture of antigen and incomplete Freund's adjuvant (Josman Labs, LLC, Napa, CA). Immune sera from the 10th week were affinity purified on the

respective antigens bound to CNBr-activated Sepharose beads (GE HealthCare, Uppsala, Sweden). HQ-Smo polyclonal antibody (pAb) 5928B antisera were generated in the same way from aggregates of unfixed antigen (because it precipitated during PBS dialysis) but were purified on a low-pH antigen-coupling resin (Actigel ALD; Sterogene, Carlsbad, CA) in PBS.

Development of anti-Gli MAbs. Ten BALB/c mice (Charles River Laboratories, Hollister, CA) were hyperimmunized six times each with a mixture of 2 μg of a 1:1 mixture of fixed and unfixed HQ-Gli antigens in Ribi adjuvant (Ribi Immunochem Research, Inc., Hamilton, MO), a mixture of the three N-terminal antigens being injected into five mice and a mixture of the three C-terminal antigens into another five mice, since the N termini were more immunogenic in rabbits. The best two mice from each group were chosen based on high anti-Gli antibody titers determined using an enzyme-linked immunosorbent assay (ELISA; plates coated with a mixture of unfixed and 1% formalin-fixed Gli antigens), as well as specific staining of transiently individually expressed myc-tagged Glis in PFA-fixed COS7 cells by IF (see below for details). B cells from the two selected mice in each group were pooled and fused with mouse myeloma cells (X63.Ag8.653; American Type Culture Collection, Rockville, MD), in a manner similar to that described previously (27, 38). After 10 to 12 days, the supernatants were harvested and screened for antibody binding by ELISA (discarding any that reacted with an irrelevant HQ-tagged protein) and IF. The positive hybridomas were subcloned twice by limiting dilution and the supernatants purified by affinity chromatography (fast protein liquid chromatography; Pharmacia, Uppsala, Sweden) as described before (27). The entire screen from mouse inoculation to selection of the final clones (of 232 initial positive parental hybridomas) took less than 11 weeks to yield 15 monoclonal antibodies (MAbs) to six different Gli antigens; thus, our cofusion and coscreening strategy was rapid as well as successful. Antibodies were sterile filtered and stored at 4°C in PBS. While all 15 MAbs and all 5 pAbs recognized their respective transfected Gli by IF and Western blotting, only the 4 MAbs and 2 pAbs that additionally recognized endogenous Gli by at least one method are characterized herein.

IF. For antibody screening, COS7 cells were transiently transfected for 48 h with full-length human myc-Gli1 (aa 2 to 1106 [78]), myc-Gli3 (aa 2 to 1596 [78]), or human myc-Gli2C (aa 827 to 1126 subcloned into pRK5 via AscI and XbaI) by using Fugene6 reagent (Roche Diagnostics, Indianapolis, IN) according to the manufacturer's protocol in 96-well black-walled microscopy plates (Whatman, Clifton, NJ). Cells were fixed with 3% PFA for 20 min at room temperature, quenched for 10 min in 50 mM NH4Cl, and permeabilized with 0.4% saponin (Sigma) in PBS containing 1% bovine serum albumin (BSA) and 2% FBS. Mouse sera were diluted 1:200 and 1:50 in saponin buffer; hybridoma supernatants were diluted 1:2. Final purified MAbs were used at 5 μg/ml, pAbs at 2 μg/ml, and 1 μg/ml anti-myc tag 9E10 (19) was a positive control. Plates were imaged with a 20× objective, using a Discovery-1 high-content screening microscope (Molecular Devices, Downingtown, PA).

For detecting cilia and endogenous Gli3 with rabbit pAbs, cells were plated in eight-well LabTekII microscope slides (Nalge Nunc, Naperville, IL), fixed and permeabilized for 4.5 min at −20°C with 100% methanol to preserve centrosomes, blocked in PBS–2% BSA–1% BSA, and stained for primary cilia with anti-acetylated tubulin MAb 6-11B-1 (Sigma) at 1:3,000, centrosomes with 1 μg/ml mouse anti-γ-tubulin MAb GTU-88 (Sigma), and 3 μg/ml rabbit anti-Gli3. Antibody staining was detected with fluorescein isothiocyanate (FITC)-labeled donkey F(ab′)2 anti-mouse heavy and light chains and the equivalent Cy3–anti-rabbit antibody (Jackson Immunoresearch, West Grove, PA). A four-step labeling protocol was employed to costain cilia with anti-Gli MAbs: (i) 1:2,000 rabbit anti-γ-tubulin (AccuSpecs, Westburg, NY) and 3 μg/ml anti-Gli MAb; (ii) FITC–anti-rabbit and Cy3–anti-mouse antibody; (iii) 10 μg/ml mouse IgG to block Cy3–anti-mouse antibody; (iv) Alexa 488 Zenon Fab anti-mouse IgG2b-labeled 6-11B-1, prepared according to the manufacturer's instructions (Molecular Probes, Carlsbad, CA). Then samples were postfixed in 3% PFA. For convenience the Gli3N polyclonal 2676 was used in all quantitative experiments after demonstrating similar results to 6F5 (see Fig. S2E in the supplemental material). Slides were coverslipped in 4′,6-diamidino-2-phenylindole (DAPI) containing Vectashield (Vector Labs, Burlingame, CA) or ProLong Gold (Invitrogen) and visualized by epifluorescence microscopy using a DeltaVision microscope (Applied Precision LLC, Issaquah, WA) powered by SoftWoRx software (version 3.4.4) and with a 60× objective. Figures were compiled using Photoshop CS software (Adobe Systems, Inc., San Jose, CA).

Measurement of ciliary Gli signals. Qualitative assessment of the strength of Gli staining at cilium tips was performed by scoring a positive signal as one that was clearly distinct from the surrounding cytoplasmic and nuclear staining in the same cell (see Fig. S2 and S3 in the supplemental material for examples). Around 200 cilia were counted for each sample, and the results are expressed as a percentage of the total cilia counted (average of three independent data sets ±

standard deviations [SDs], unless otherwise specified). P values for n independent replicate experiments were calculated online using the unpaired t test with $n - 1$ degrees of freedom (GraphPad).

Quantitative analysis of Gli signal per cilium was performed using ImageJ software (version 1.41; W. Rasband, NIH) by drawing an eight-by-eight circle around the cilium tips in the acetylated tubulin channel and measuring the integrated density in the Gli channel within the same area. The mean fluorescence intensity of all the cilia in one image was averaged with that of all the other images in the same experiment, and SDs across all images were calculated.

siRNA transfection. Pools of predesigned On-Target-Plus small interfering RNAs (siRNAs) for murine Gli2, Gli3, Smo, SPOP, Cul1, Cul3, IFT88, and Dynch21 or siGenome siRNAs for mouse βTrCP and Kif3a were purchased from Dharmacon Inc. (Lafayette, CO). S12 cells were seeded into eight-well LabTekII microscope slides at 3×10^4 cells/well or into six-well plates at 3×10^5 cells/well and reverse transfected with 100 nM final siRNA pools, following a 20-min preincubation of 1 nmol siRNA and 30 μl DharmaFECT-2 (Dharmacon) in Optimem (Gibco) at room temperature. After 48 h, cells were shifted into 0.5% FBS medium for an additional 16 h to promote ciliation (with or without Hh for the indicated times).

Immunoprecipitation and Western blot assays. Cells were serum starved to induce ciliation for 16 to 24 h with or without 10 μM MG132 (CalBiochem 474790), 100 nM HhAntag (21), 20 μM cell permeant PKA inhibitor (myristoylated 14-22 amide; CalBiochem 476485), 10 μM H-89 (Calbiochem 371963), 10 μM KT5720 (Calbiochem 420320), or 40 μM forskolin (Calbiochem 344270), all with or without Hh. Cell extracts were prepared by lysing EDTA-detached cells with radioimmunoprecipitation assay (RIPA) buffer (50 mM Tris [pH 7.5], 150 mM NaCl, 1 mM EDTA, 1% Triton X-100, 0.1% SDS, 1% sodium deoxycholate) containing freshly added phosphatase inhibitor cocktails I and II (P-2850 and P-5726; Sigma), Complete protease inhibitor cocktail (Roche), and 1 mM phenylmethylsulfonyl fluoride (PMSF; Sigma) on ice for 30 min. Insoluble debris was removed by centrifugation at $16,000 \times g$ for 20 min at 4°C.

Lysate concentrations were determined with the bicinchoninic acid (BCA) kit (Pierce, Rockford, IL) and compared to BSA standards in RIPA buffer, and the samples were equalized with RIPA buffer. Two-milligram aliquots of lysates were precleared with 50 μl of 50% (vol/vol) protein G-Sepharose beads, then incubated with 2 μg of pAb or 5 μg of MAb for 1 h at 4°C, and then overnight with 50 μl preequilibriated 50% protein G-Sepharose beads (GE HealthCare) on a rotator. Immunoprecipitates (washed five times) and lysates were boiled in Lane Maker sample reducing buffer (Thermo Scientific, Waltham, MA) for 5 min at 94°C, and half the immunoprecipitates or 30-μg aliquots of the lysates were separated on a 4 to 12% Tris-glycine SDS-PAGE (unless otherwise specified) with Precision Plus protein standards (Bio-Rad, Hercules, CA) and transferred to nitrocellulose membranes (all reagents from Invitrogen, Carlsbad, CA). Membranes were incubated with 2 to 5 μg/ml anti-Gli antibodies in 5% (wt/vol) milk in Tris-buffered saline–0.05% Tween 20 followed by horseradish peroxidase (HRP)-conjugated secondary antibodies. Endogenous Gli bands were visualized with ChemiGlow substrate (Alpha Innotech, San Leandro, CA), while overexpressed myc-Gli and full-length human Gli2-myc-FLAG (Origene RC217291; Fugene6-transfected into 293 cells as above) and tubulin controls (1: 10,000 dilution of 1A2 MAb; Sigma T9028) were visualized with ECL reagent (GE HealthCare). Except where otherwise labeled (in Fig. 1 below and Fig. S1 in the supplemental material), MAb 6F5 was used for all Gli3 Western blot assays.

Real-time qPCR. Total RNA was extracted from cells using the RNeasy Protect minikit (Qiagen, Valencia, CA) according to the manufacturer's protocol. On-column genomic DNA digestion was performed with an RNase-free DNase set (Qiagen). cDNA synthesis from total RNA was conducted using the High Capacity reverse transcription kit (Applied Biosystems, Foster City, CA) with random hexamer primers. Quantitative PCRs (qPCRs) were performed in triplicate on a Prism 7500 sequence detection system (Applied Biosystems) using murine ribosomal protein L19 (mRPL19) as the endogenous control. Gene expression was calculated using the relative quantification ($2^{-\Delta\Delta Ct}$) method. PCR primers and TaqMan probes are listed in Table S1 of the supplemental material.

RESULTS

Generation of antibodies recognizing endogenous Gli2 and Gli3. To detect endogenous Glis and to differentiate between full-length protein and the N-terminal repressor, we raised rabbit pAbs and mouse MAbs to the N and C termini of Gli1,
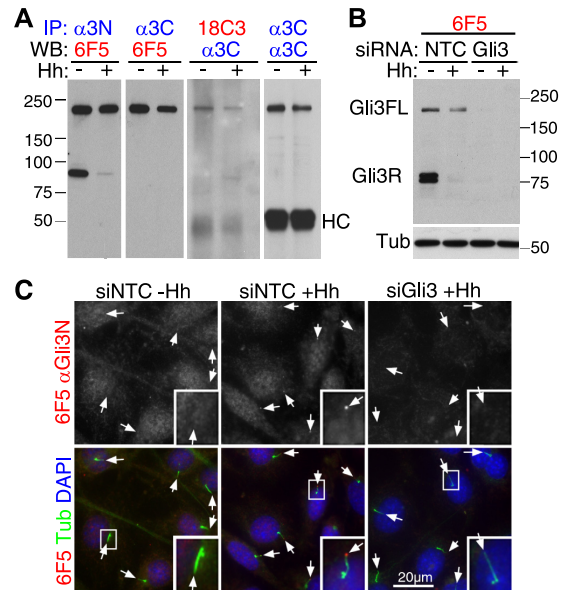

FIG. 1. Detection of endogenous Gli3 in S12 cells. (A) Endogenous Gli3 can be immunoprecipitated and detected by Western blotting. Extracts of S12 cells treated for 16 h with (+) or without (-) Hh were immunoprecipitated (IP) with anti-Gli3N pAb, anti-Gli3C pAb, or MAb 18C3 and Western blotted (WB) with anti-Gli3N MAb 6F5 or anti-Gli3C pAb as indicated (pAbs are shown in blue and MAb clones are in red). Molecular mass markers in kDa are indicated on the left. HC, antibody heavy chain. (B) 6F5 anti-Gli3N MAb is specific for Gli3. Extracts of S12 cells transfected with nontargeting control (NTC) or Gli3 siRNAs with or without Hh treatment for 16 h were Western blotted with 6F5. Tub, antitubulin loading control. (C) Immunofluorescence detection of endogenous Gli3. S12 cells transfected with nontargeting control (siNTC) or Gli3 (siGli3) siRNAs with or without 30-min Hh stimulation were costained with 6F5 (red channel and upper panels), cilia and centrosomes (anti-acetylated tubulin and anti-γ-tubulin, respectively (Tub) (green channel), and DAPI (blue channel) for nuclei. Arrows indicate cilium tips. Bar, 20 μm. Insets show 3× magnifications of the boxed regions.

-2, and -3. We identified three antibodies that detected the N terminus of Gli3 (Gli3N), pAb 2676 and MAbs 6F5 and 20B7, two antibodies to the Gli3 C terminus (Gli3C), pAb 2438 and MAb 18C3, and one antibody to the Gli2 C terminus (Gli2C), MAb 1H6. All six Abs specifically detected their cognate transfected antigens by IF and Western blotting (see Fig. S1 in the supplemental material).

We found that Gli3 immunoprecipitated from ciliated S12 cell extracts with either Gli3N or Gli3C pAbs was readily detected by MAb 6F5 as an ~190-kDa full-length band (Fig. 1A), as seen in mouse embryos with other anti-Gli3 pAbs (41, 87). As expected, the Gli3N but not the Gli3C pAb pulled down the processed N terminus of Gli3 (Gli3R) at ~83 kDa only in the absence of Hh. Immunoprecipitation using Gli3C MAb or pAb pulled down Gli3FL but not a cleavage product of the expected size for the Gli3 C terminus (~107 kDa), suggesting that the C terminus is rapidly degraded in the absence of Hh signaling, as is that of Ci in *Drosophila* (4), as previously hypothesized (57, 83).

Furthermore, Gli3N MAbs 6F5 and 20B7 could detect endogenous Gli3 in extracts of ciliated S12, 3T3, and MEF cells without prior enrichment by immunoprecipitation (Fig. 1B and
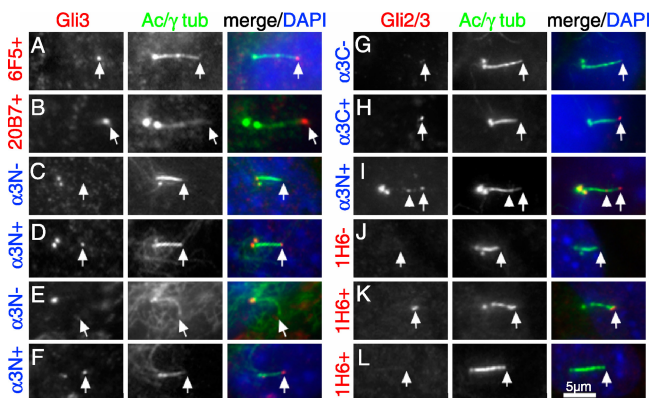
FIG. 2. Gli3 and Gli2 accumulate at cilium tips in response to Hh in multiple cell lines. IMCD3 (A, B, and G to I), 3T3 (C and D), primary E10.5 MEF (E and F), or S12 (J to L) cells were treated for 16 h in the absence or presence of Hh and costained with various antibodies to Gli3 or Gli2 in the red channel (left), acetylated tubulin (cilia) and γ-tubulin (centrosomes) together in the green channel (middle), and merged with DAPI (blue) on the right. (A and B) Gli3N MAb 6F5 (A) and 20B7 (B) staining of IMCD3 cells with Hh. (C to F) Gli3N pAb 2676 staining of 3T3 (C and D) and MEF (E and F) cells with or without Hh treatment; pAb 2676 also nonspecifically stains the centrosome (see Fig. S2C and D in the supplemental material). (G and H) Anti-Gli3C pAb 2438 staining of IMCD3 cells with or without Hh. An additional Gli3 spot (arrowhead) along the cilium (I), here in IMCD3 cells in the presence of Hh. (J to L) Anti-Gli2C MAb 1H6 staining of S12 cells without Hh (J), with Hh (K), and with Hh after Gli2 siRNA transfection (L). pAbs are labeled alongside in blue, and MAbs are in red, with + or - indicating the presence or absence of Hh, respectively. White arrows indicate cilium tips.

data not shown), with a stronger signal and fewer background bands than all published antibodies (1, 11, 15, 28, 42, 51, 81, 87). As previously observed (42, 87), in the absence of Hh Gli3R sometimes appears as a doublet (p83 and p75), possibly a result of alternative cleavage or degradation stop sites during proteasomal degradation of the C terminus (57, 83). All three bands are specific, as they were abolished by siRNA knockdown of Gli3 (Fig. 1B).

Full-length Gli3 and Gli2 accumulate at tips of cilia in multiple cell types upon Hh stimulation. Gli3 and Gli2 are found at the tips of cilia in cultured murine limb bud cells (25), human embryonic stem cells (36), and MEF and 3T3 cells (12, 52), requiring Hh stimulation in the latter two cell types (18). To determine if Gli3 ciliary localization is also Hh dependent in S12 cells, we stained them with Gli3N MAb 6F5, which detects both Gli3FL and Gli3R. Indeed, Gli3 accumulated at distal tips of cilia in up to 80% of cells following Hh stimulation (Fig. 1C; see also Fig. S2E in the supplemental material). Additionally, we observed faint cytoplasmic puncta and a stronger nuclear signal, which, like the cilium staining, were specific since they disappeared following Gli3 siRNA treatment (Fig. 1C) or preincubation of the antibody with Gli3N (see Fig. S2D). The nuclear signal is likely predominantly Gli3R, since it mostly disappeared following overnight Hh stimulation (see Fig. S1F), when Gli3R is virtually absent (Fig. 1B).

Similar Hh-dependent ciliary tip staining was found in IMCD3, 3T3, and MEF cells (Fig. 2A to F) and with both of the Gli3N Abs (Fig. 2B to F). Importantly, the Hh-stimulated

ciliary tip staining was also seen with anti-Gli3C (Fig. 2G and H), indicating accumulated ciliary Gli3 is likely full-length, in agreement with the inhibition of Gli3 processing by Hh and the lack of Gli3R-green fluorescent protein in cilia (25, 51). Occasionally Gli3 appeared as more than one spot, as if fixed in transit to or from the cilium tip (Fig. 2I).

Anti-Gli2C MAb 1H6 recognizes transfected Gli2 (see Fig. S1C in the supplemental material), but not endogenous Gli2 (data not shown), by Western blotting. However, it similarly stained the tips of cilia upon Hh stimulation, and this signal disappeared following siRNA knockdown of Gli2 (Fig. 2J to L), suggesting Hh-accumulated ciliary Gli2 is similarly full-length.

Hh-promoted ciliary localization of Gli3 and Gli2 is rapid and requires active Smo. To further characterize Hh-regulated Gli3 and Gli2 accumulation in cilia, we quantitated it (see Fig. S3 in the supplemental material for details). We found only ~10% of S12 cells had ciliary Gli3 or Gli2 in the absence of Hh, while overnight Hh stimulation increased this to >50% (Fig. 3A). Primary MEFs gave similar results, although the basal ciliary levels of both Glis were higher, likely reflecting the higher levels of endogenous Hh detected in these cells (see Fig. S4A to C). Since Ptch exits and Smo enters cilia within 1 h of Hh stimulation in MEFs (13, 65), we expected that Gli2 and Gli3, as downstream effectors of Smo, would follow a similar temporal trend of ciliary accumulation in S12 cells. Surprisingly, however, Gli3 accumulated at the cilium tip as quickly as 5 to 10 min after Hh addition, peaking at ~80% cilia in 30 to 60 min and declining somewhat thereafter, reaching a plateau of 50 to 60% (Fig. 3B; see also Fig. S3A in the supplemental material). We also measured the average fluorescence intensity of Gli3 per cilium in the same set of images and found good correlation at each time point, except at 0 to 5 min and at 18 h, when the fluorescence intensity measurements were slightly higher (Fig. 3C). This validates our less-time-consuming qualitative scoring method, which was used in all further experiments. Gli2 was similarly first enriched within 5 min, peaked at 30 min in ~50% of cilia, and then declined with similar kinetics to Gli3, except it increased again after 2 h (Fig. 3B and D), probably due to Hh-dependent stabilization (56), as *Gli2* mRNA was not upregulated until >16 h (Fig. 3E). The average fluorescence intensity of Gli2 per cilium also correlated with the overall percentage of positive cilia, except for being slightly lower at the 18-h time point (Fig. 3D).

To determine if Smo follows the same kinetics, we generated a rabbit pAb that recognizes endogenous ciliary Smo (see Fig. S5 in the supplemental material) and confirmed that, as in MEFs, Smo is not significantly enriched in S12 cilia until ≥60 min after Hh addition, continuing to accumulate over 18 h to ~70% of cilia (Fig. 3B). This is likely due to insufficient sensitivity of the anti-Smo antibody, because knocking down or inactivating Smo (with siRNAs [20] or the small-molecule inhibitors HhAntag [21, 67] and cyclopamine [9], respectively) prevented Gli3 accumulation following 30 min of subsequent Hh treatment, indicating active Smo as well as Hh is required for Gli3 accumulation (Fig. 3F; see also Fig. S2F to K in the supplemental material). Smo knockdown similarly inhibited Gli2 accumulation in cilia (Fig. 3F). As Smo inactivation also decreased the basal levels of ciliary Gli, endogenous Hh (Ihh or Dhh) (see Fig. S4) is likely responsible for the low levels of
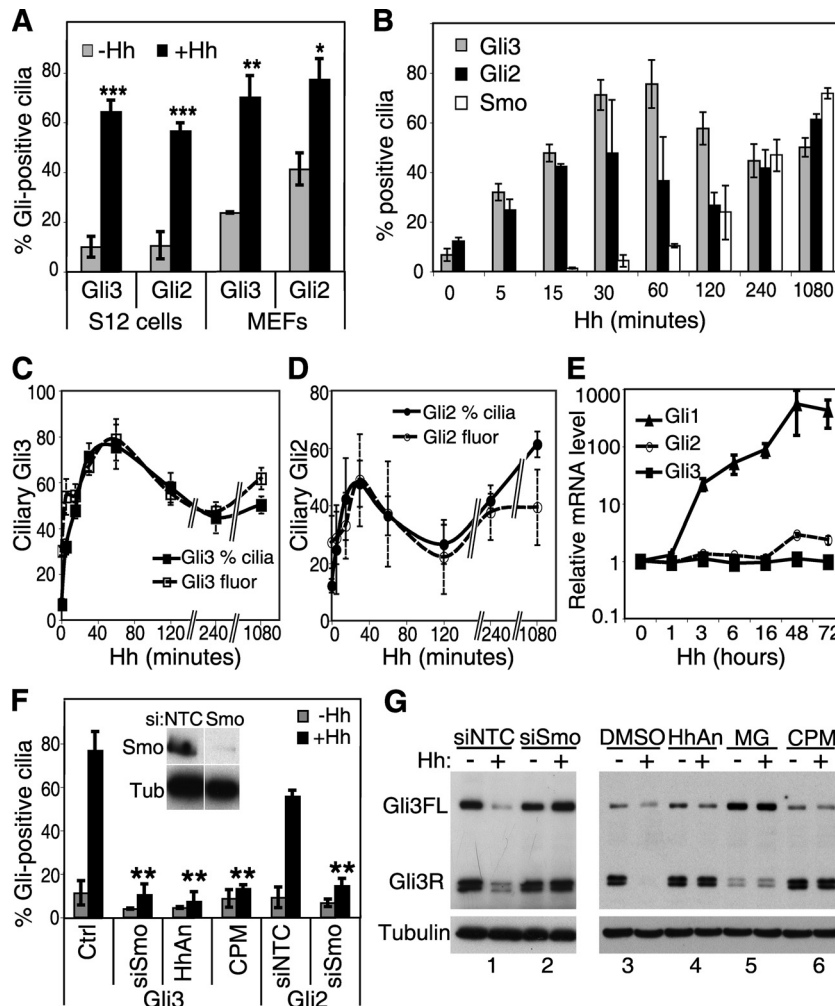
FIG. 3. Gli3 and Gli2 accumulation at cilium tips is rapid and requires active Smo. (A) Quantitation of Gli3 and Gli2 accumulation at cilium tips following Hh stimulation. S12 cells and E10.5 MEFs were treated for 24 h with or without Hh, then stained for cilia, centrosomes, and Gli3 (2676) or Gli2 (1H6). At least 150 cilia were scored (as in Fig. S3 of the supplemental material) in each of three (MEF) or five (S12) independent experiments, and the mean ± SD was plotted. Asterisks denote statistical significance between experiments with and without Hh according to the t test. $*$, $P \leq 0.05$; $**$, $P \leq 0.01$; $***$, $P \leq 0.001$. (B) Time course of Hh-dependent Gli and Smo ciliary accumulation. S12 cells stimulated with Hh for the indicated times were stained for Gli2 (1H6) or Gli3 (2676) and quantitated as for panel A. Smo (5928B) was stained and quantitated as for Fig. S5C in the supplemental material. (C) Correlation between ciliary Gli3 qualitative scoring method used for panel B and quantitative fluorescence intensities measured with ImageJ (arbitrary fluorescence units divided by 30 to fit on the same scale). (D) Same experiment as for panel C, except this experiment compared ciliary Gli2 qualitative (●) and quantitative (○; 1.15×) signals. (E) *Gli3* mRNA levels are not altered by Hh stimulation. S12 cells were treated with Hh for the indicated times, and then *Gli1*, *Gli2*, and *Gli3* mRNA levels were assessed by qPCR, normalized to RPL19, and expressed relative to unstimulated cells. *Gli3* did not show any significant change, but *Gli1* was upregulated by Hh as expected. Data are the means and SD of two to four independent experiments for each time point. (F) Active Smo is required for Hh-dependent Gli3 and Gli2 accumulation at cilium tips. NTC siRNA- or Smo siRNA-transfected S12 cells were treated with or without Hh for 30 min. Alternatively, S12 cells were treated for 1 h with DMSO, 100 nM HhAntag (HhAn), or 5 μM cyclopamine (CPM) with or without Hh for the final 30 min. Ciliary Gli3 or Gli2 was quantitated as for panel B in two independent experiments of ≥200 cilia. siNTC and DMSO gave similar results for Gli3, and so the combined data are shown (Ctrl). $**$, $P \leq 0.01$ versus Hh-treated control. The inset is a 14A5 MAb Western blot of Smo knockdown versus siNTC with tubulin loading controls (Tub). (G) Smo knockdown or inactivation prevents Hh-mediated inhibition of Gli3 processing and degradation. S12 cells were treated as for panel F, except that Hh and drug treatments were for 16 h, and then blotting was performed with 6F5 as for Fig. 1B. Lanes: 1, nontargeting control siRNA; 2, Smo siRNA; 3, DMSO control; 4, 100 nM HhAntag; 5,10 μM MG132; 6, 5 μM cyclopamine.

ciliary Gli2 and Gli3 under unstimulated conditions. Thus, it is probable that Smo is translocated at the same time as or prior to Gli2 and Gli3 but is simply more difficult to detect, being spread all along the cilium, compared to the concentrated single spot of Gli at the tip. While we cannot exclude that Smo acts catalytically in cilia, similar to the inhibition of Smo itself by Ptch (79), we think this unlikely, as the ~10% Smo protein

remaining after knockdown (Fig. 3F, inset) was insufficient to permit Gli accumulation. Interestingly, while cyclopamine enriched Smo in primary cilia in the absence of Hh, consistent with recent findings (64, 91, 93), HhAntag did not (see Fig. S5D in the supplemental material), suggesting that this inhibitor must stabilize a different, nonciliary conformation of Smo than cyclopamine. Since both compounds inhibit signaling un-

der these conditions (96), accumulation of Smo in cilia *per se* cannot be sufficient for subsequent Gli2 and Gli3 accumulation; rather, Smo must accumulate in its active form, as occurs during Hh stimulation. Alternatively, it is possible that a minimal level of active Smo protein is required, but its detectable localization to cilia is not a prerequisite for Gli accumulation.

Smo knockdown or inactivation also prevented Hh from inhibiting Gli3 processing (Fig. 3G), retaining both Gli3FL and Gli3R at levels similar to those under nonstimulated conditions. Surprisingly, while Hh stimulation in control cells inhibited Gli3 processing as expected (15, 42, 87), this did not result in increased levels of Gli3FL, instead consistently decreasing them, an effect that also required active Smo (Fig. 3G). While Hh inhibits *Gli3* transcription in chick limb buds, as seen with *in situ* hybridization (74) and in micromass cultures by Northern blotting (87), qPCR revealed no changes in S12 cell *Gli3* mRNA over 72 h of Hh treatment that could account for the loss of Gli3FL using any of three independent primer/probe sets (Fig. 3E and data not shown). Rather, the Hh-mediated decline in Gli3FL is due to posttranslational degradation, as it was prevented by the proteasomal inhibitor MG132 (Fig. 3G), which also inhibited processing, as expected.

Gli3FL and Gli3R are proteasomally degraded with distinct kinetics. To further understand Gli3 processing and degradation, we compared Gli3 levels over a time course of Hh and/or MG132 treatment, especially since IF revealed that ciliation was disrupted after 16 h of MG132 treatment (data not shown). We found that the levels of Gli3FL decreased as early as 1 h post-Hh treatment (when cells and cilia appeared normal), with an apparent half-life of ~2 h under our blotting conditions (Fig. 4A and C). However, Gli3FL did not completely disappear, reaching a minimum plateau of ~30% after 6 h. Proteasome inhibition with MG132 alone slightly increased the basal levels of Gli3FL, consistent with inhibition of Gli3 processing. Importantly, MG132 also inhibited the Hh-dependent degradation of Gli3FL at all time points (Fig. 4A and C), confirming that this is due to proteasomal degradation and not loss of cilia.

By comparison, the Hh-dependent disappearance of Gli3R was about twice as slow as that of Gli3FL (apparent $t_{1/2}$, ~4 h) (Fig. 4A and D; see also Fig. S6A in the supplemental material) but did continue to completion, with no detectable Gli3R remaining after 16 h of Hh treatment at this exposure level (Fig. 4A and D). This was likely a combination of proteasomal degradation and inhibited formation via Gli3 processing, because adding MG132 together with Hh retarded the disappearance of Gli3R at the same rate as MG132 alone. It is possible that Hh and MG132 similarly inhibit the *de novo* formation of Gli3R (by inhibiting Gli3FL processing). However, it is not possible to distinguish whether Hh has no effect on the degradation of preexisting Gli3R or if it accelerates it via a proteasomal pathway.

To confirm that this was not an artifact of MG132 treatment, we compared Gli3 levels over a time course of Hh treatment with that of the protein synthesis inhibitor cycloheximide (CHX). Gli3FL disappeared much faster upon treatment with Hh than with CHX (Fig. 4B and E), confirming it is posttranslationally degraded upon Hh stimulation. CHX did not increase the rate of the Hh-mediated disappearance of Gli3FL. Gli3R remained stable for ≥6 h under nonstimulated condi-

tions (CHX alone), and interestingly, adding CHX to the Hh treatment actually inhibited the disappearance of Gli3R compared to Hh alone (Fig. 4B and F; see also Fig. S6 in the supplemental material), suggesting that the proteins that mediate Gli3R degradation may themselves be short-lived (turned over within 3 h) and that their identities may be different from those mediating Gli3FL degradation (see below).

Full-length Hh-activated Gli3 is degraded by the SPOP/Cul3 complex. In the developing eye of *Drosophila* Hh-activated CiFL (CiA) is labile and proteasomally degraded in the nucleus via binding to HIB (97), also known as Roadkill (35), in a complex with the Cul3 ubiquitin ligase (55). Mammalian SPOP (speckle type POZ protein) is 79% identical to HIB and can functionally substitute for it in degrading Ci *in vivo*, as well as degrading ectopically expressed Gli2 and Gli3 (97). We therefore asked whether SPOP and Cul3 could be the E3 ligase responsible for the lability of Gli3FL in Hh-stimulated S12 cells. Indeed, siRNA-mediated knockdown of either SPOP (by 80% at the mRNA level) or to a lesser extent Cul3 (by 70%) stabilized Gli3FL 5- to 6-fold in the presence of Hh relative to the nontargeting control (Fig. 4G; see also Fig. S8A and B in the supplemental material). Importantly, Gli3FL was stabilized relatively more in the presence than absence of Hh, leading us to speculate that the nonphosphorylated form of Gli3FL may be the preferred substrate of SPOP. (The 1.4-fold increase in Gli3FL without Hh likely reflects the portion of Gli3FL activated by endogenous Hh.) This is consistent with the ability of HIB to degrade a non-PKA-phosphorylatable mutant of Ci and its preference for CiA over CiFL (97). Unlike *HIB*, however, *SPOP* itself was not significantly upregulated by Hh stimulation at this time point (see Fig. S8A).

Gli3 processing in the absence of Hh was not inhibited by loss of SPOP/Cul3 but was inhibited by loss of βTrCP and the SCF complex component Cul1, as expected from earlier results with transfected Gli3 (81, 88). Both Gli3FL and Gli3FL:R ratios (Fig. 4H) increased more with knockdown of Cul1 (by ~75% at the mRNA level) than with βTrCP, which we could not silence to >50% without inducing toxicity (see Fig. S8C and D in the supplemental material). Note that unlike with MG132 (Fig. 4A and D), Gli3R completely disappeared after 16-h Hh treatment in the absence of either SPOP/Cul3 or βTrCP/Cul1 complexes, suggesting that yet another E3 ligase complex promotes its proteasomal degradation. This would be consistent with our above hypothesis that the mediators of Gli3R degradation are short-lived (<3 h), since the half-life of Cul3 is as long as 6 h in MEFs (48) and similar to that of Cul1 in *Drosophila* larval cells (95). Taken together, these results support the hypothesis (97) that the function of HIB/SPOP is conserved from flies to mammals, degrading unphosphorylated Gli3FL in the presence of Hh, while the βTrCP/Cul1 complex processes phosphorylated Gli3FL into Gli3R in the absence of Hh.

Inhibition of Gli3FL degradation increases the levels of ciliary Gli3. The above results suggest that Hh-activated Gli3 is labile because SPOP degrades presumably unphosphorylated Gli3FL in an Hh-dependent manner. Since Hh also accumulates Gli3FL at cilium tips (Fig. 2H), we speculated that increasing the available pool of Gli3FL by SPOP knockdown would result in accumulation of ciliary Gli3 in an Hh-dependent manner. Indeed, siRNAs to SPOP (and to a lesser extent Cul3) did cause a small but reproducible increase in the per-
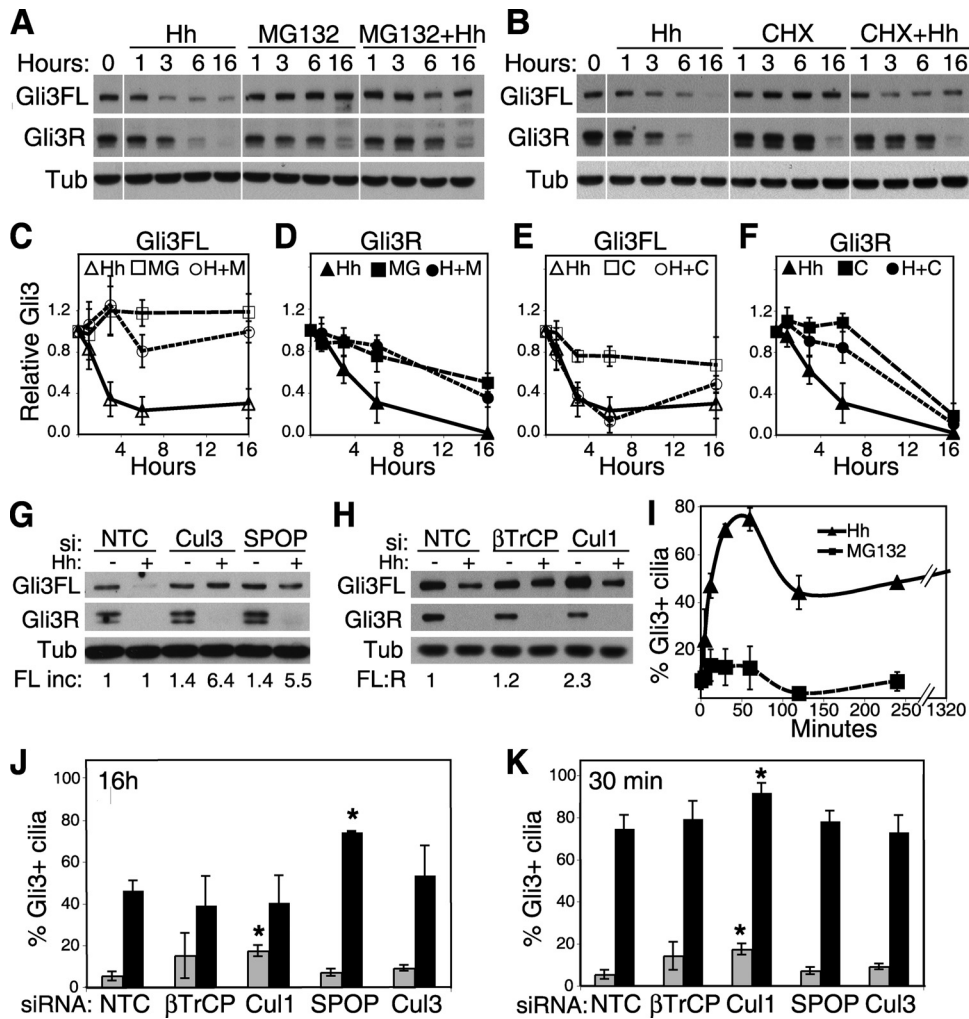
FIG. 4. Gli3FL and Gli3R are processed and degraded by independent proteasomal pathways. (A) Gli3 Western blotting time course of MG132 with and without Hh treatment. S12 cells were serum starved for 16 h alone (0) or with Hh, 10 μM MG132, or both for 1, 3, 6, or 16 h and then blotted with 6F5 as described for Fig. 1B. The blot shown is representative of ≥6 experiments, with white lines drawn between different treatments. The empty blot between Gli3FL and Gli3R was excised to save space. (B) Gli3 Western blotting time course of cycloheximide with or without Hh treatment. The experiment was similar to that in panel A, except 10 μg/ml CHX replaced MG132. The single blot shown is representative of four experiments, with white lines separating treatments. (C and D) Quantitation of Gli3 levels in panel A. Gli3FL (C) and Gli3R (D) bands were normalized to the tubulin loading controls and plotted relative to untreated cells, assigned a value of 1 (means and SDs of 6 to 10 experiments, one of which is shown in panel A). H+M, Hh and MG132. For easier comparisons of Gli3FL and Gli3R, combined graphs are presented in Fig. S6 of the supplemental material. (E and F) Quantitation of Gli3 levels in panel B. The same experiment was performed as in panels C and D, except CHX (C) replaced MG132; data shown are from four experiments (10 for Hh), one being shown in panel B. C, CHX only; H+C, Hh and CHX. See also Fig. S6A, D, and E in the supplemental material. (G) SPOP or Cul3 knockdown inhibits the Hh-induced degradation of Gli3FL without affecting processing. S12 cells transfected with siRNAs to SPOP or Cul3 were treated for 16 h in the presence or absence of Hh and then blotted as described for panel A. The mean increase in Gli3FL relative to siNTC with or without Hh from three independent blots is shown underneath this representative blot. (H) βTrCP or Cul1 knockdown inhibits Gli3R formation while permitting Hh-dependent degradation of Gli3FL. The experiment was similar to that shown in panel G, except siRNAs were to βTrCP or Cul1. The mean Gli3FL:R ratio of two blots relative to siNTC without Hh is shown underneath (the absence of Gli3R with Hh precluded ratio calculations). (I) Time course of Gli3 accumulation in cilia with MG132 treatment. S12 cells treated with Hh or MG132 for different times were stained for ciliary Gli3 (2676 pAb) and quantitated as in Fig. S2 of the supplemental material. No cilia remained after 16 h of MG132 treatment, so that the curve ends at 6 h. (J and K) Knockdown of E3 ligases increases Gli3-positive cilia. S12 cells transfected with siRNAs to βTrCP, Cul1, SPOP, or Cul3 were treated with or without Hh for 16 h (J) or 30 min (K), stained, and quantitated as for panel I. The mean and SD of two to three independent experiments is shown. ∗, $P \leq 0.05$.

centage of Gli3-positive cilia after 16 h of Hh treatment, compared to control Hh-stimulated cells (Fig. 4J) and, as expected, this depended on the presence of Hh. More strikingly, an ~2-fold increase in average Gli3 fluorescence intensity per cilium was observed compared to control cells (see Fig. S7 in the supplemental material), supporting our hypothesis that

unphosphorylated Gli3FL may be the accumulated species. As expected from the 2-h half-life of Gli3FL in the presence of Hh (Fig. 4C), 30 min of Hh stimulation was not sufficient to accumulate this extra ciliary Gli3 in SPOP-deficient cells (Fig. 4K).

To confirm that Hh is required for ciliary Gli3 accumulation and that mere accumulation of Gli3FL by inhibiting its pro-

cessing or degradation with MG132 is not sufficient, we compared ciliary Gli3 following Hh or MG132 treatment. At no time point could MG132 substitute for Hh in accumulation of ciliary Gli3 (Fig. 4I); thus, Hh activation is essential, and so we speculate that it is Gli3A rather than Gli3FL that accumulates in cilia.

Enhanced ciliary Gli3 was also observed following enrichment of Gli3FL with siRNAs to Cul1 (and to a lesser extent βTrCP, again likely due to less efficient knockdown) (Fig. 4J and K). However, unlike SPOP knockdown, a slight increase also occurred in the absence of Hh, since Gli3FL already accumulates in the absence of Hh via inhibited processing (Fig. 4H). A small but significant increase in *Gli1* levels in the absence of Hh resulted from knockdown of βTrCP/Cul1 as well as with SPOP (see Fig. S8A to D in the supplemental material); thus, these results can likely be explained either by accumulation of Gli3A (activated by endogenous Hh) or by pathway derepression due to loss of Gli3R. However, the enhanced ciliary accumulation of Gli3FL under Hh-stimulated conditions did not lead to significantly greater *Gli1* transcription compared to Hh-stimulated cells with intact E3 ligases. This suggests either that Gli3A is not the major transcriptional activator of *Gli1* in S12 cells (perhaps because it is degraded too quickly, as *Gli1* is not elevated until 3 h of Hh stimulation [Fig. 3E]) or that ciliary Gli3FL, while unphosphorylated, is not the functional equivalent of Gli3A. Nonetheless, the levels of ciliary Gli3 do mirror the subsequent levels of *Gli1* transcript, but they are elevated more rapidly in response to Hh.

PKA-phosphorylated Gli3 does not accumulate in primary cilia. The βTrCP/SCF complex is specific for Gli3 phosphorylated by PKA/CK1/GSK3β in the absence of Hh (88), while HIB (and presumably SPOP) can bind and mediate degradation of unphosphorylated CiA (32, 97). Since Hh stimulation is required for both Gli3FL accumulation in cilia and SPOP-mediated degradation, we hypothesized that ciliary Gli3 should be non-PKA phosphorylated. To test this, we examined whether accumulation or depletion of PKA-phosphorylated Gli3 (using the PKA stimulator FSK or PKA inhibitors) prevented or enhanced Gli3 accumulation in cilia, respectively.

The efficacies of FSK and three different PKA inhibitors, H-89, KT5720, and myristoylated 14-22 amide, were first verified by testing their effects on Gli3 processing. As expected, FSK stimulated Gli3 processing irrespective of Hh treatment, as previously shown (81, 88). The possibility that FSK simply stabilizes preexisting Gli3R rather than stimulating processing *per se* was ruled out by its lack of effect in Cul1-depleted cells (see Fig. S8G in the supplemental material). Conversely, all three PKA inhibitors inhibited Gli3 processing and accumulated Gli3FL (Fig. 5A; see also Fig. S8H in the supplemental material). Further experiments utilized myristoylated 14-22 amide (henceforth abbreviated as PKAi) due to its higher potency and greater PKA selectivity. Neither FSK nor PKAi affected *Gli3* mRNA levels, confirming that these changes are posttranscriptional (see Fig. S8E). Furthermore, consistent with PKA being a known negative regulator of the mammalian Hh pathway (24, 75, 90), the 4-h FSK treatment inhibited Hh-induced *Gli1* transcription as well as decreasing basal levels by ~40% (see Fig. S8F). Conversely, PKAi caused a small but significant upregulation of *Gli1* mRNA (see Fig. S8F), likely due to pathway derepression induced by loss of Gli3R.
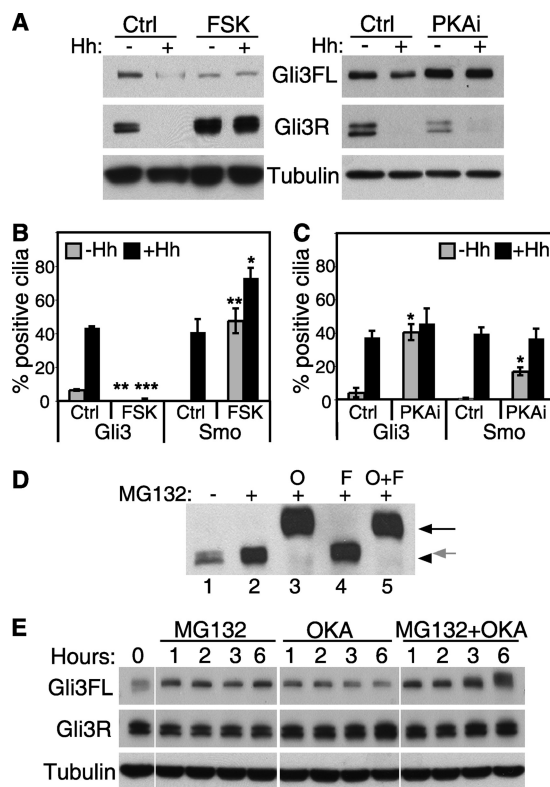

FIG. 5. Ciliary Gli3 is not PKA phosphorylated and is processed or dynamically dephosphorylated. (A) FSK stimulates Gli3 processing and the PKA inhibitor myristoylated 14-22 amide (PKAi) prevents it. 6F5 blots of S12 cells treated for 16 h with 40 μM FSK or vehicle (Ctrl) with or without Hh (left panel) or 20 μM PKAi or vehicle (Ctrl) with or without Hh (right panel). (B) FSK inhibits Hh-dependent accumulation of Gli3 but not Smo in cilia. Cells were treated for 4 h with 40 μM FSK or vehicle (Ctrl) in the absence of presence of Hh, then stained and scored for ciliary Gli3 (2676, left) or Smo (right) as in Fig. 3B (mean and SD of two independent experiments). *, $P \leq 0.05$; **, $P \leq 0.01$; ***, $P \leq 0.001$ versus the corresponding control with or without Hh. (C) PKA inhibition results in Hh-independent accumulation of Gli3 and Smo in cilia. An experiment similar to that in panel B was performed, except 20 μM PKAi replaced FSK. (D) Endogenous Gli3 is dynamically phosphorylated and dephosphorylated. Extracts of S12 cells treated for 16 h (+) or not (-) with 10 μM MG132 and 100 nM okadaic acid (O; lane 3), 40 μM forskolin (F; lane 4), or both (lane 5) were run on a 4% SDS-PAGE gel and blotted with 6F5. Black arrowhead, Gli3FL; gray arrow, presumptive phospho-Gli3FL; black arrow, presumptive hyperphosphorylated Gli3FL. (E) At least 3 h is required to accumulate hyperphosphorylated Gli3 in the absence of proteasomal activity. Four to 12% 6F5 blots of S12 cells treated for the indicated times with 10 μM MG132, 100 nM OKA, or both. The samples are all on the same blot, with vertical lines drawn for easier viewing.

As predicted, phosphorylation of Gli3 via FSK treatment completely abolished its accumulation in cilia, both with and without concomitant addition of Hh for 30 min (data not shown) or for 4 h (Fig. 5B), even though Gli3FL is still abundant at these time points (data not shown). Conversely, 4-h PKAi treatment led to accumulated Gli3 in cilia even without Hh treatment and to a similar level as Hh treatment alone (Fig. 5C). Hh stimulation was not additive with PKA inhibition with respect to either the percentage of Gli3-positive cilia or the stimulation of *Gli1* transcription (Fig.

5C; see also Fig. S8F in the supplemental material). This confirms that non-PKA-phosphorylated Gli3 preferentially accumulates in cilia and that one role of Hh is to antagonize PKA activity toward Gli3 (87), as previously proposed for Ci activation (90). This does not mean, however, that PKA phosphorylation of Gli3 does not occur in cilia, just that phospho-Gli3 does not accumulate at cilium tips.

Because FSK inhibits Gli3 accumulation as early as 30 min (prior to any detectable changes in *Gli1* transcription), we wanted to determine whether this was due to inhibited translocation of Smo. Unlike Gli3, however, Smo did accumulate all along cilia after a 4-h FSK treatment, to a comparable level as with Hh treatment, and was further enhanced by Hh treatment (Fig. 5B). This confirms previous observations that FSK inhibition of pathway activity occurs downstream of Smo translocation: Chuang et al. reported similar results in MEF cilia after overnight FSK incubation (93), although by that time point Smo accumulated only at the base of (not all along) the cilium, which they hypothesized to be inactive Smo. The base of the cilium cannot be the only location of inactive Smo, however, since cyclopamine-inactivated Smo accumulates all along the cilium (64, 91, 93) (see Fig. S5D in the supplemental material). Furthermore, Smo also showed significant ciliary accumulation in PKAi-treated cells, although to a lesser extent than with Hh or FSK stimulation (Fig. 5C). Thus, while it is unclear whether Smo all along cilia after FSK treatment is active or not, ciliary Gli3 clearly only accumulates when not PKA phosphorylated.

Phospho-Gli3 is dephosphorylated or processed. To examine whether PKA-phosphorylated Gli3 is stable in the absence of Hh, we attempted to enrich it with FSK or the protein phosphatase inhibitor okadaic acid (OKA), both in the presence of MG132 to suppress any processing of phospho-Gli3. Immunoblotting with 6F5 on a low-percentage gel permitted resolution of a doublet of Gli3FL in the absence of MG132, presumptively unphosphorylated and phosphorylated Gli3 (although other posttranslational modifications are also possible), both bands of which were stabilized by MG132 (Fig. 5D, lanes 1 and 2). Addition of OKA caused a marked decrease in electrophoretic mobility (lane 3), while FSK did not unless OKA was also present (lanes 4 and 5). Combined with the knowledge that FSK must effectively stimulate the Gli3 phosphorylation cascade, because it efficiently stimulated Gli3 processing (Fig. 5A), these data imply the existence of robust phosphatase activity (in the absence of OKA). Although we cannot exclude the presence of additional modifications, such as ubiquitination during OKA treatment, these data are consistent with the known accumulation of hyperphosphorylated Ci by OKA (8) and imply that Gli3FL can be similarly hyperphosphorylated but subject to rapid processing or dephosphorylation by an OKA-sensitive phosphatase, such as PP2A (31). The OKA-induced retardation of migration in the presence of MG132 was detectable as early as 3 h of treatment and was not observed in the absence of MG132, due to enhanced processing (Fig. 5E). Taken together, these results suggest that Gli3 is dynamically phosphorylated and either processed or dephosphorylated and that non-PKA-phosphorylated Gli3FL preferentially accumulates in cilia upon Hh stimulation.

IFT is required for efficient Gli3 degradation as well as processing. Gli3 processing is thought to require cilia, or at least intact IFT machinery, as Gli3R formation is impaired in
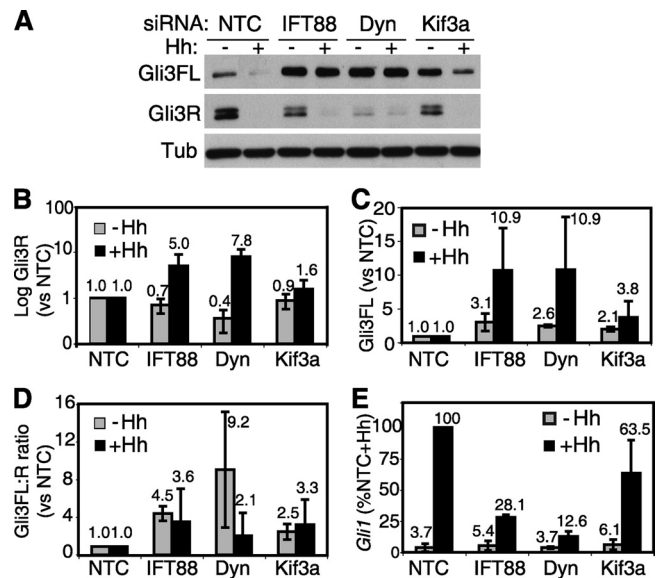

FIG. 6. IFT and microtubules are required for both processing and degradation of Gli3FL. (A) Knockdown of IFT components inhibits both Gli3FL processing and degradation. Shown is a 6F5 blot of S12 cells transfected with siRNAs to the NTC, IFT88, Dync2h1 (Dyn), or Kif3a and treated for 16 h in the presence of absence of Hh. (B) Quantitation of Gli3R relative to siNTC from three blots, with a representative one shown in panel A. Note that the log scale better reveals the decrease in Gli3R upon *ift* knockdown. (C) Quantitation of Gli3FL in the same three blots as in panel B. (D) Gli3FL:R ratios from panels B and C, normalized to 1 for siNTC. (E) *Gli1* levels measured by qPCR and normalized to siNTC plus Hh (16 h) as 100%.

a variety of *ift* mutant mice, resulting in an increased Gli3FL:R ratio and polydactyly in limb buds (16, 28, 29). However, our discovery of the Hh-induced lability of Gli3FL makes it possible that this increased ratio could be at least partly due to inefficient SPOP-mediated Gli3FL degradation. To determine if this is the case, we knocked down the anterograde IFT component IFT88 (25, 29, 43) and the anterograde and retrograde motors Kif3a and Dync2h1 (28, 47), respectively, with siRNA and examined Gli3 levels with or without Hh treatment. Kif3a knockdown was not very effective and so had less of an effect on signaling, as assessed by Hh-stimulated *Gli1* upregulation (Fig. 6E), than the ≥70% knockdown levels of Dync2h1 and IFT88 (see Fig. S8I in the supplemental material). As previously reported, in the absence of Hh disruption of the latter two IFT components decreased production of Gli3R by up to 60% (Fig. 6A and B) and increased Gli3FL levels by ~3-fold (Fig. 6C). As predicted, in the presence of Hh, Gli3FL levels were indeed also elevated, by >10 times compared to control siRNA-treated cells, consistent with impaired degradation in activated IFT-depleted cells. Thus, both inhibition of Gli3R formation and inhibition of Gli3FL degradation contribute to the increased Gli3FL:R ratios under these conditions (Fig. 6D) and likely also in *ift* mutant mouse limb buds, given the known expression of Hh there (7).

DISCUSSION

We have shown here using four new antibodies capable of detecting endogenous Gli3 that this transcription factor local-

izes to the tips of primary cilia within 5 to 10 min of Hh stimulation in four different cell lines. The ciliary Gli3 is full-length, non-PKA phosphorylated, and depends on active Smo as well as Hh. Full-length Gli2 also accumulates in cilia with similar kinetics in a Smo- and Hh-dependent fashion. The relative Gli2 and Gli3 accumulation levels upon Hh stimulation are greater in cells expressing low levels of endogenous Hh (like S12 cells) than in those with higher levels of Hh (like MEFs), which might explain why ciliary Gli3 appeared to be Hh independent in the Hh-expressing limb bud cultures, where Gli3 was first seen in cilia (25). During review of this report, Chuang and colleagues reported similar Hh-stimulated endogenous Gli3 and Gli2 accumulation in MEF cilia by using independent antibodies (10), corroborating our results.

Our findings that ciliary Gli3 is full-length and requires both Hh and lack of PKA phosphorylation are consistent with previous proposals that activation of Gli3FL into Gli3A occurs via anterograde transport into cilia (28, 84). Full-length Gli2 also accumulates in cilia in an Hh-dependent fashion with similar kinetics and may similarly be activated into Gli2A at cilium tips because in *alien* mutant mice (mutated in *thm1/ift139*) it accumulates there due to impaired retrograde IFT, leading to ventralized neural tubes characteristic of excessive Gli2A activity (84). An activation step other than inhibition of PKA phosphorylation is also likely because although non-PKA-phosphorylatable mutants of Gli2 and Gli3 (P1 to P4) exhibit constitutive activity, both require Hh for full activation *in vivo* (58, 89).

In the absence of Hh, low basal levels of Gli2 and Gli3 are seen at cilium tips, likely at least partly due to endogenous Hh signaling, since their levels decrease upon Smo inhibition. However, it is also possible that Gli2 and Gli3 constitutively cycle through cilia at low levels, as has been proposed for Smo itself (54), and that the rate of ciliary entry increases or ciliary exit decreases upon Hh stimulation. Alternatively the rate-limiting step in Gli2 and Gli3 translocation could be during the switch from anterograde to retrograde IFT, resulting in transient accumulation that permits an Hh-dependent activating modification. Or, something could specifically tether activated Gli2 and Gli3 at cilium tips. Such a tether is unlikely to be Smo, because it accumulates all along the cilia, not just at tips, in response to Hh.

Since PKA has been localized to cilia (46, 60, 71), while the downstream kinases CK1ε and GSK3β (23, 77) and ubiquitin ligase components βTrCP, Skp1, and Cul1 are all found at centrosomes (22, 63), the simplest working model for Hh-dependent Gli3 accumulation is as presented in Fig. 7. In the absence of Hh, low levels of Gli3FL cycle in and out of cilia via IFT, becoming phosphorylated by PKA but not accumulating at cilium tips (Fig. 7A). Upon returning to the centrosome at the base of the cilia, phospho-Gli3 is further phosphorylated by GSK3β and CK1ε, becoming a substrate for βTrCP/Cul1 ubiquitination and processing into Gli3R by the proteasome, a portion of which is also found at centrosomes (92). Gli3R then translocates to the nucleus to inhibit Hh target gene expression prior to being degraded by an unknown E3 ligase complex. We suspect that the nuclear Gli3 signal detected with anti-Gli3N MAb 6F5 is mainly Gli3R, because it mostly disappears following overnight Hh treatment, when little Gli3R remains (see Fig. S1F in the supplemental material), although it is not yet
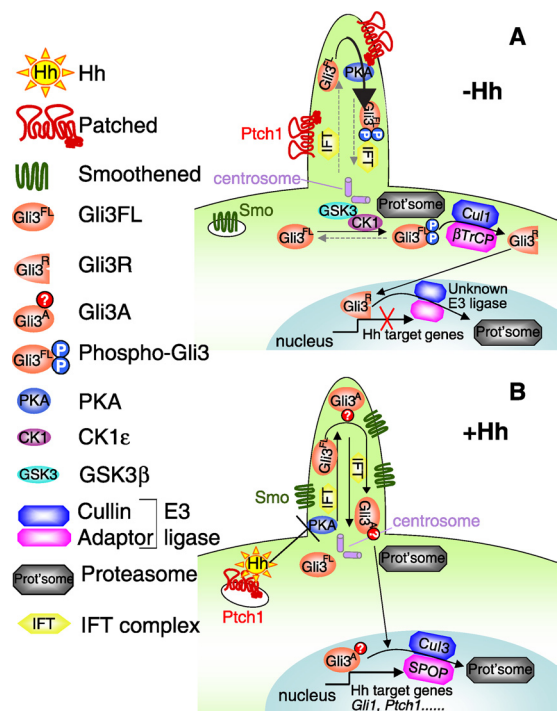

FIG. 7. Working model for Gli3 translocation, processing, and degradation. (A) In the absence of Hh, Ptch, but not Smo, is present in cilia, and Gli3 (and Gli2) may translocate at low levels into and out of cilia (denoted by dashed arrows), where PKA could phosphorylate them. However, cilia are not absolutely required for Gli3 processing, so PKA phosphorylation could also occur in the cytoplasm, priming Glis for further phosphorylation by centrosomal CK1ε and GSK3β. Phosphorylated Gli3 binds the centrosomal βTrCP/Cul1 complex, becoming ubiquitinated and processed by the pericentrosomal proteasome into Gli3R, which presumably translocates to the nucleus to inhibit transcription by Gli2 and Gli1 prior to degradation by an unknown E3 ligase complex. (B) In the presence of Hh, Smo replaces Ptch in cilia and Gli3FL (and Gli2FL) accumulate at the distal tips via IFT (denoted by solid arrows). PKA phosphorylation is inhibited, preventing βTrCP/Cul1 binding and processing. We propose an as-yet unidentified modification (red circle) occurs at cilium tips to activate the Gli3 (into Gli3A), which not only prevents it from being processed, but also permits subsequent transport to the nucleus to allow activation of transcription of Hh target genes, including *Gli1* and *Ptch1*. Following this, Gli3A is ubiquitinated by the SPOP/Cul3 complex and degraded by the proteasome.

clear whether the rate of Gli3R degradation *per se* (as opposed to inhibited formation) is affected by Hh.

In the presence of Hh (Fig. 7B), PKA is inhibited, preventing the Gli3 phosphorylation cascade and permitting unphosphorylated Gli3FL to accumulate at cilium tips, where we propose yet-to-be determined modifications activate it into Gli3A. While Gli3 accumulation can be detected faster than the exchange of Ptch1 for Smo in cilia (65), it does depend on active Smo. We speculate that Gli3A then translocates to the nucleus, consistent with the notion that it can act as a transcriptional activator (76) and is rapidly degraded ($t_{1/2}$ of ~2 h in S12 cells) by the SPOP/Cul3 complex and nuclear proteasomes (5), perhaps explaining its relatively minor contribution to *Gli1* transcription in these cells. Our proposed degradation of Gli3A by SPOP/Cul3 is analogous to that of CiA by the HIB/Cul3 complex in *Drosophila*. Like HIB, endogenous mam-

malian SPOP localizes to nuclear speckles (50) and can recruit Cul3 from the cytoplasm along with degradation substrates (40), likely including Gli3. Other scenarios for Gli3 phosphorylation and its inhibition by Hh are also possible, including Hh-regulated relocalization to cilia of one or more of the kinase or E3 ligase components themselves.

Our finding that endogenous Gli3FL (or Gli3A) is degraded by endogenous SPOP in an Hh-dependent manner is in partial agreement with recent findings by Chuang and colleagues, who showed that overexpressed Gli3FL (and Gli2FL) could be degraded by overexpressed SPOP (10), albeit in large cytoplasmic "blobs" reminiscent of inclusion bodies rather than in the nucleus. However, they did not find degradation to be Hh dependent, perhaps because overexpression disrupts Hh regulation; indeed, transfected Gli accumulates in cilia without Hh (10, 25). Alternatively, the higher endogenous Hh levels in MEFs may obscure the Hh dependence of SPOP degradation, although exogenous Hh still promotes ciliary accumulation of endogenous Gli in these cells.

Our results also have implications for understanding the role of cilia in Gli3 function. While IFT renders Gli3 processing more efficient, perhaps by concentrating Gli3 together with PKA or other enzymes in cilia, accumulation of Gli3 in cilia *per se* appears not to be absolutely required for processing. For example, Gli3R formation occurred under conditions of Smo inhibition or FSK treatment, when Gli3 does not accumulate in cilia (although Gli3 could still transit through cilia undetected). Since PKA is present in nonciliated organisms and is not restricted to cilia, it is highly probable that some (maybe less efficient) phosphorylation and processing of Gli3 can occur without cilia. Indeed, every Gli3 Western blot assay of cilia-deficient *ift* mutant mice has shown Gli3R is only diminished, not absent (14, 25, 28, 29, 43, 47). Furthermore, our finding that Gli3FL becomes more labile upon Hh stimulation (unless IFT or SPOP is disrupted) suggests that at least some of the increased Gli3FL:R ratio in *ift* mutants is due to impaired activation and SPOP-mediated degradation rather than solely due to impaired processing.

It should be noted that the Gli3 spot at the tip of cilia at any one time is only a small fraction (likely less than 0.01%) of the total Gli3 seen on a Western blot. The small fraction of Gli3 in cilia makes it unlikely that Gli3 is simply protected from centrosomal processing by sequestration at cilium tips in the presence of Hh. It may also explain the disconnect between the rapid ciliary accumulation in minutes and prominent Gli3 band intensity changes in hours. It has recently been proposed that SuFu may regulate Gli2 and Gli3 stability by competing for SPOP downstream of cilia altogether (10).

In summary, our novel antibodies recognizing endogenous Gli2 and Gli3 are valuable tools for better understanding the Hh pathway, and the Gli ciliary accumulation assay can be used to decipher Hh signaling events upstream of Gli. We recently found that Kif7, which itself concentrates at cilium tips upon Hh stimulation, is required for maximal levels of Gli accumulation per cilium (18), although it does not affect the overall percentage of positive cilia. However, many questions remain to be addressed, including how Gli2 and Gli3 accumulate at cilium tips upon Hh stimulation, what happens to activate them there, and how their transport to the nucleus from the cilium and their subsequent degradation is regulated. Dyrk2

phosphorylates Gli2 and Gli3 and induces their degradation (85), so it would be interesting to see if this kinase is ciliary or affects Gli translocation. Alternatively, a phosphatase antagonizing PKA upon Hh stimulation could act in cilia to prevent Gli3 processing, so investigation of PP2A, shown in *Drosophila* to dephosphorylate Ci (31) and found in motile cilia (60), may be warranted. Furthermore, the precise roles and Hh-dependent localization of several other genes required for signaling between Hh/Smo and Gli3 proteins, including Tulp3 (52, 59), Rab23 (17), Tectonic (61), and Arl13b (6), remain to be determined. Our Gli2 and Gli3 ciliary accumulation assay should be a useful tool for probing such questions.

REFERENCES

1. **Agren, M., P. Kogerman, M. I. Kleman, M. Wessling, and R. Toftgard.** 2004. Expression of the PTCH1 tumor suppressor gene is regulated by alternative promoters and a single functional Gli-binding site. Gene **330**:101–114.
2. **Alexandre, C., A. Jacinto, and P. W. Ingham.** 1996. Transcriptional activation of Hedgehog target genes in Drosophila is mediated directly by the cubitus interruptus protein, a member of the GLI family of zinc finger DNA-binding proteins. Genes Dev. **10**:2003–2013.
3. **Aza-Blanc, P., H. Y. Lin, A. Ruiz i Altaba, and T. B. Kornberg.** 2000. Expression of the vertebrate Gli proteins in Drosophila reveals a distribution of activator and repressor activities. Development **127**:4293–4301.
4. **Aza-Blanc, P., F. A. Ramirez-Weber, M. P. Laget, C. Schwartz, and T. B. Kornberg.** 1997. Proteolysis that is inhibited by Hedgehog targets Cubitus interruptus protein to the nucleus and converts it to a repressor. Cell **89:** 1043–1053.
5. **Brooks, P., G. Fuertes, R. Z. Murray, S. Bose, E. Knecht, M. C. Rechsteiner, K. B. Hendil, K. Tanaka, J. Dyson, and J. Rivett.** 2000. Subcellular localization of proteasomes and their regulatory complexes in mammalian cells. Biochem. J. **346**:155–161.
6. **Caspary, T., C. E. Larkins, and K. V. Anderson.** 2007. The graded response to Sonic Hedgehog depends on cilia architecture. Dev. Cell **12**:767–778.
7. **Chang, D. T., A. Lopez, D. P. von Kessler, C. Chiang, B. K. Simandl, R. Zhao, M. F. Seldin, J. F. Fallon, and P. A. Beachy.** 1994. Products, genetic linkage and limb patterning activity of a murine Hedgehog gene. Development **120**:3339–3353.
8. **Chen, C. H., D. P. von Kessler, W. Park, B. Wang, Y. Ma, and P. A. Beachy.** 1999. Nuclear trafficking of Cubitus interruptus in the transcriptional regulation of Hedgehog target gene expression. Cell **98**:305–316.
9. **Chen, J. K., J. Taipale, M. K. Cooper, and P. A. Beachy.** 2002. Inhibition of Hedgehog signaling by direct binding of cyclopamine to Smoothened. Genes Dev. **16**:2743–2748.
10. **Chen, M. H., C. W. Wilson, Y. J. Li, K. K. Law, C. S. Lu, R. Gacayan, X. Zhang, C. C. Hui, and P. T. Chuang.** 2009. Cilium-independent regulation of Gli protein function by Sufu in Hedgehog signaling is evolutionarily conserved. Genes Dev. **23**:1910–1928.
11. **Chen, Y., V. Knezevic, V. Ervin, R. Hutson, Y. Ward, and S. Mackem.** 2004. Direct interaction with Hoxd proteins reverses Gli3-repressor function to promote digit formation downstream of Shh. Development **131**:2339–2347.
12. **Cho, A., H. W. Ko, and J. T. Eggenschwiler.** 2008. FKBP8 cell-autonomously controls neural tube patterning through a Gli2- and Kif3a-dependent mechanism. Dev. Biol. **321**:27–39.
13. **Corbit, K. C., P. Aanstad, V. Singla, A. R. Norman, D. Y. Stainier, and J. F. Reiter.** 2005. Vertebrate Smoothened functions at the primary cilium. Nature **437**:1018–1021.
14. **Cortellino, S., C. Wang, B. Wang, M. R. Bassi, E. Caretti, D. Champeval, A. Calmont, M. Jarnik, J. Burch, K. S. Zaret, L. Larue, and A. Bellacosa.** 2009. Defective ciliogenesis, embryonic lethality and severe impairment of the Sonic Hedgehog pathway caused by inactivation of the mouse complex A

intraflagellar transport gene Ift122/Wdr10, partially overlapping with the DNA repair gene Med1/Mbd4. Dev. Biol. **325**:225–237.

15. **Dai, P., H. Akimaru, Y. Tanaka, T. Maekawa, M. Nakafuku, and S. Ishii.** 1999. Sonic Hedgehog-induced activation of the Gli1 promoter is mediated by GLI3. J. Biol. Chem. **274**:8143–8152.

16. **Eggenschwiler, J. T., and K. V. Anderson.** 2007. Cilia and developmental signaling. Annu. Rev. Cell Dev. Biol. **23**:345–373.

17. **Eggenschwiler, J. T., O. V. Bulgakov, J. Qin, T. Li, and K. V. Anderson.** 2006. Mouse Rab23 regulates Hedgehog signaling from smoothened to Gli proteins. Dev. Biol. **290**:1–12.

18. **Endoh-Yamagami, S., M. Evangelista, D. Wilson, X. Wen, J.-W. Theunissen, K. Phamluong, M. Davis, S. J. Scales, M. J. Solloway, F. J. de Sauvage, and A. S. Peterson.** 2009. The mammalian Cos2 homolog Kif7 plays an essential role in modulating Hh signal transduction during development. Curr. Biol. **19**:1320–1326.

19. **Evan, G. I., G. K. Lewis, G. Ramsay, and J. M. Bishop.** 1985. Isolation of monoclonal antibodies specific for human c-myc proto-oncogene product. Mol. Cell. Biol. **5**:3610–3616.

20. **Evangelista, M., T. Y. Lim, J. Lee, L. Parker, A. Ashique, A. S. Peterson, W. Ye, D. P. Davis, and F. J. de Sauvage.** 2008. Kinome siRNA screen identifies regulators of ciliogenesis and hedgehog signal transduction. Sci. Signal **1**:ra7.

21. **Frank-Kamenetsky, M., X. M. Zhang, S. Bottega, O. Guicherit, H. Wichterle, H. Dudek, D. Bumcrot, F. Y. Wang, S. Jones, J. Shulok, L. L. Rubin, and J. A. Porter.** 2002. Small-molecule modulators of Hedgehog signaling: identification and characterization of Smoothened agonists and antagonists. J. Biol. **1**(2):10.

22. **Freed, E., K. R. Lacey, P. Huie, S. A. Lyapina, R. J. Deshaies, T. Stearns, and P. K. Jackson.** 1999. Components of an SCF ubiquitin ligase localize to the centrosome and regulate the centrosome duplication cycle. Genes Dev. **13**:2242–2257.

23. **Fumoto, K., C. C. Hoogenraad, and A. Kikuchi.** 2006. GSK-3β-regulated interaction of BICD with dynein is involved in microtubule anchorage at centrosome. EMBO J. **25**:5670–5682.

24. **Hammerschmidt, M., M. J. Bitgood, and A. P. McMahon.** 1996. Protein kinase A is a common negative regulator of Hedgehog signaling in the vertebrate embryo. Genes Dev. **10**:647–658.

25. **Haycraft, C. J., B. Banizs, Y. Aydin-Son, Q. Zhang, E. J. Michaud, and B. K. Yoder.** 2005. Gli2 and Gli3 localize to cilia and require the intraflagellar transport protein polaris for processing and function. PLoS Genet **1**:e53.

26. **Hill, P., K. Gotz, and U. Ruther.** 2009. A SHH-independent regulation of Gli3 is a significant determinant of anteroposterior patterning of the limb bud. Dev. Biol. **328**:506–516.

27. **Hongo, J. A., M. Mora-Worms, C. Lucas, and B. M. Fendly.** 1995. Development and characterization of murine monoclonal antibodies to the latency-associated peptide of transforming growth factor beta 1. Hybridoma **14**:253–260.

28. **Huangfu, D., and K. V. Anderson.** 2005. Cilia and Hedgehog responsiveness in the mouse. Proc. Natl. Acad. Sci. U. S. A. **102**:11325–11330.

29. **Huangfu, D., A. Liu, A. S. Rakeman, N. S. Murcia, L. Niswander, and K. V. Anderson.** 2003. Hedgehog signalling in the mouse requires intraflagellar transport proteins. Nature **426**:83–87.

30. **Ingham, P. W., and A. P. McMahon.** 2001. Hedgehog signaling in animal development: paradigms and principles. Genes Dev. **15**:3059–3087.

31. **Jia, H., Y. Liu, W. Yan, and J. Jia.** 2009. PP4 and PP2A regulate Hedgehog signaling by controlling Smo and Ci phosphorylation. Development **136**:307–316.

32. **Jiang, J.** 2006. Regulation of Hh/Gli signaling by dual ubiquitin pathways. Cell Cycle **5**:2457–2463.

33. **Jiang, J., and C. C. Hui.** 2008. Hedgehog signaling in development and cancer. Dev. Cell **15**:801–812.

34. **Kalderon, D.** 2000. Transducing the Hedgehog signal. Cell **103**:371–374.

35. **Kent, D., E. W. Bush, and J. E. Hooper.** 2006. Roadkill attenuates Hedgehog responses through degradation of Cubitus interruptus. Development **133**:2001–2010.

36. **Kiprilov, E. N., A. Awan, R. Desprat, M. Velho, C. A. Clement, A. G. Byskov, C. Y. Andersen, P. Satir, E. E. Bouhassira, S. T. Christensen, and R. E. Hirsch.** 2008. Human embryonic stem cells in culture possess primary cilia with Hedgehog signaling machinery. J. Cell Biol. **180**:897–904.

37. **Kirchhofer, D., M. Peek, W. Li, J. Stamos, C. Eigenbrot, S. Kadkhodayan, J. M. Elliott, R. T. Corpuz, R. A. Lazarus, and P. Moran.** 2003. Tissue expression, protease specificity, and Kunitz domain functions of hepatocyte growth factor activator inhibitor-1B (HAI-1B), a new splice variant of HAI-1. J. Biol. Chem. **278**:36341–36349.

38. **Kohler, G., and C. Milstein.** 1975. Continuous cultures of fused cells secreting antibody of predefined specificity. Nature **256**:495–497.

39. **Kozminski, K. G., K. A. Johnson, P. Forscher, and J. L. Rosenbaum.** 1993. A motility in the eukaryotic flagellum unrelated to flagellar beating. Proc. Natl. Acad. Sci. U. S. A. **90**:5519–5523.

40. **Kwon, J. E., M. La, K. H. Oh, Y. M. Oh, G. R. Kim, J. H. Seol, S. H. Baek, T. Chiba, K. Tanaka, O. S. Bang, C. O. Joe, and C. H. Chung.** 2006. BTB domain-containing speckle-type POZ protein (SPOP) serves as an adaptor

41. **Litingtung, Y., and C. Chiang.** 2000. Specification of ventral neuron types is mediated by an antagonistic interaction between Shh and Gli3. Nat. Neurosci. **3**:979–985.

42. **Litingtung, Y., R. D. Dahn, Y. Li, J. F. Fallon, and C. Chiang.** 2002. Shh and Gli3 are dispensable for limb skeleton formation but regulate digit number and identity. Nature **418**:979–983.

43. **Liu, A., B. Wang, and L. A. Niswander.** 2005. Mouse intraflagellar transport proteins regulate both the activator and repressor functions of Gli transcription factors. Development **132**:3103–3111.

44. **Lum, L., and P. A. Beachy.** 2004. The Hedgehog response network: sensors, switches, and routers. Science **304**:1755–1759.

45. **Marigo, V., R. L. Johnson, A. Vortkamp, and C. J. Tabin.** 1996. Sonic Hedgehog differentially regulates expression of GLI and GLI3 during limb development. Dev. Biol. **180**:273–283.

46. **Masyuk, A. I., S. A. Gradilone, J. M. Banales, B. Q. Huang, T. V. Masyuk, S. O. Lee, P. L. Splinter, A. J. Stroope, and N. F. Larusso.** 2008. Cholangiocyte primary cilia are chemosensory organelles that detect biliary nucleotides via P2Y12 purinergic receptors. Am. J. Physiol. Gastrointest. Liver Physiol. **295**:G725–G734.

47. **May, S. R., A. M. Ashique, M. Karlen, B. Wang, Y. Shen, K. Zarbalis, J. Reiter, J. Ericson, and A. S. Peterson.** 2005. Loss of the retrograde motor for IFT disrupts localization of Smo to cilia and prevents the expression of both activator and repressor functions of Gli. Dev. Biol. **287**:378–389.

48. **McEvoy, J. D., U. Kossatz, N. Malek, and J. D. Singer.** 2007. Constitutive turnover of cyclin E by Cul3 maintains quiescence. Mol. Cell. Biol. **27**:3651–3666.

49. **McMahon, A. P., P. W. Ingham, and C. J. Tabin.** 2003. Developmental roles and clinical significance of Hedgehog signaling. Curr. Top. Dev. Biol. **53**:1–114.

50. **Nagai, Y., T. Kojima, Y. Muro, T. Hachiya, Y. Nishizawa, T. Wakabayashi, and M. Hagiwara.** 1997. Identification of a novel nuclear speckle-type protein, SPOP. FEBS Lett. **418**:23–26.

51. **Nielsen, S. K., K. Mollgard, C. A. Clement, I. R. Veland, A. Awan, B. K. Yoder, I. Novak, and S. T. Christensen.** 2008. Characterization of primary cilia and Hedgehog signaling during development of the human pancreas and in human pancreatic duct cancer cell lines. Dev. Dyn. **237**:2039–2052.

52. **Norman, R. X., H. W. Ko, V. Huang, C. M. Eun, L. L. Abler, Z. Zhang, X. Sun, and J. T. Eggenschwiler.** 2009. Tubby-like protein 3 (TULP3) regulates patterning in the mouse embryo through inhibition of Hedgehog signaling. Hum. Mol. Genet. **18**:1740–1754.

53. **Nybakken, K., and N. Perrimon.** 2002. Hedgehog signal transduction: recent findings. Curr. Opin. Genet. Dev. **12**:503–511.

54. **Ocbina, P. J., and K. V. Anderson.** 2008. Intraflagellar transport, cilia, and mammalian Hedgehog signaling: analysis in mouse embryonic fibroblasts. Dev. Dyn. **237**:2030–2038.

55. **Ou, C. Y., Y. F. Lin, Y. J. Chen, and C. T. Chien.** 2002. Distinct protein degradation mechanisms mediated by Cul1 and Cul3 controlling Ci stability in Drosophila eye development. Genes Dev. **16**:2403–2414.

56. **Pan, Y., C. B. Bai, A. L. Joyner, and B. Wang.** 2006. Sonic Hedgehog signaling regulates Gli2 transcriptional activity by suppressing its processing and degradation. Mol. Cell. Biol. **26**:3365–3377.

57. **Pan, Y., and B. Wang.** 2007. A novel protein-processing domain in Gli2 and Gli3 differentially blocks complete protein degradation by the proteasome. J. Biol. Chem. **282**:10846–10852.

58. **Pan, Y., C. Wang, and B. Wang.** 2009. Phosphorylation of Gli2 by protein kinase A is required for Gli2 processing and degradation and the Sonic Hedgehog-regulated mouse development. Dev. Biol. **326**:177–189.

59. **Patterson, V. L., C. Damrau, A. Paudyal, B. Reeve, D. T. Grimes, M. E. Stewart, D. J. Williams, P. Siggers, A. Greenfield, and J. N. Murdoch.** 2009. Mouse hitchhiker mutants have spina bifida, dorso-ventral patterning defects and polydactyly: identification of Tulp3 as a novel negative regulator of the Sonic Hedgehog pathway. Hum. Mol. Genet. **18**:1719–1739.

60. **Porter, M. E., and W. S. Sale.** 2000. The 9 + 2 axoneme anchors multiple inner arm dyneins and a network of kinases and phosphatases that control motility. J. Cell Biol. **151**:F37–F42.

61. **Reiter, J. F., and W. C. Skarnes.** 2006. Tectonic, a novel regulator of the Hedgehog pathway required for both activation and inhibition. Genes Dev. **20**:22–27.

62. **Riobo, N. A., and D. R. Manning.** 2007. Pathways of signal transduction employed by vertebrate Hedgehogs. Biochem. J. **403**:369–379.

63. **Rogers, G. C., N. M. Rusan, D. M. Roberts, M. Peifer, and S. L. Rogers.** 2009. The SCF Slimb ubiquitin ligase regulates Plk4/Sak levels to block centriole reduplication. J. Cell Biol. **184**:225–239.

64. **Rohatgi, R., L. Milenkovic, R. B. Corcoran, and M. P. Scott.** 2009. Hedgehog signal transduction by Smoothened: pharmacologic evidence for a 2-step activation process. Proc. Natl. Acad. Sci. U. S. A. **106**:3196–3201.

65. **Rohatgi, R., L. Milenkovic, and M. P. Scott.** 2007. Patched 1 regulates Hedgehog signaling at the primary cilium. Science **317**:372–376.

66. **Rohatgi, R., and M. P. Scott.** 2007. Patching the gaps in Hedgehog signalling. Nat. Cell Biol. **9**:1005–1009.

of Daxx for ubiquitination by Cul3-based ubiquitin ligase. J. Biol. Chem. **281**:12664–12672.

67. Romer, J. T., H. Kimura, S. Magdaleno, K. Sasai, C. Fuller, H. Baines, M. Connelly, C. F. Stewart, S. Gould, L. L. Rubin, and T. Curran. 2004. Suppression of the Shh pathway using a small molecule inhibitor eliminates medulloblastoma in Ptc1$^{+/-}$ p53$^{-/-}$ mice. Cancer Cell 6:229–240.

68. Ruiz i Altaba, A., C. Mas, and B. Stecca. 2007. The Gli code: an information nexus regulating cell fate, stemness and cancer. Trends Cell Biol. 17:438–447.

69. Ruppert, J. M., K. W. Kinzler, A. J. Wong, S. H. Bigner, F. T. Kao, M. L. Law, H. N. Seuanez, S. J. O'Brien, and B. Vogelstein. 1988. The GLI-Kruppel family of human genes. Mol. Cell. Biol. 8:3104–3113.

70. Ruppert, J. M., B. Vogelstein, K. Arheden, and K. W. Kinzler. 1990. GLI3 encodes a 190-kilodalton protein with multiple regions of GLI similarity. Mol. Cell. Biol. 10:5408–5415.

71. Salathe, M. 2007. Regulation of mammalian ciliary beating. Annu. Rev. Physiol. 69:401–422.

72. Sasaki, H., Y. Nishizaki, C. Hui, M. Nakafuku, and H. Kondoh. 1999. Regulation of Gli2 and Gli3 activities by an amino-terminal repression domain: implication of Gli2 and Gli3 as primary mediators of Shh signaling. Development 126:3915–3924.

73. Scales, S. J., and F. J. de Sauvage. 2009. Mechanisms of Hedgehog pathway activation in cancer and implications for therapy. Trends Pharmacol. Sci. 30:303–312.

74. Schweitzer, R., K. J. Vogan, and C. J. Tabin. 2000. Similar expression and regulation of Gli2 and Gli3 in the chick limb bud. Mech. Dev. 98:171–174.

75. Sheng, T., S. Chi, X. Zhang, and J. Xie. 2006. Regulation of Gli1 localization by the cAMP/protein kinase A signaling axis through a site near the nuclear localization signal. J. Biol. Chem. 281:9–12.

76. Shin, S. H., P. Kogerman, E. Lindstrom, R. Toftgard, and L. G. Biesecker. 1999. GLI3 mutations in human disorders mimic Drosophila cubitus interruptus protein functions and localization. Proc. Natl. Acad. Sci. U. S. A. 96:2880–2884.

77. Sillibourne, J. E., D. M. Milne, M. Takahashi, Y. Ono, and D. W. Meek. 2002. Centrosomal anchoring of the protein kinase CK1δ mediated by attachment to the large, coiled-coil scaffolding protein CG-NAP/AKAP450. J. Mol. Biol. 322:785–797.

78. Stone, D. M., M. Murone, S. Luoh, W. Ye, M. P. Armanini, A. Gurney, H. Phillips, J. Brush, A. Goddard, F. J. de Sauvage, and A. Rosenthal. 1999. Characterization of the human suppressor of Fused, a negative regulator of the zinc-finger transcription factor Gli. J. Cell Sci. 112:4437–4448.

79. Taipale, J., M. K. Cooper, T. Maiti, and P. A. Beachy. 2002. Patched acts catalytically to suppress the activity of Smoothened. Nature 418:892–897.

80. Taylor, F. R., D. Wen, E. A. Garber, A. N. Carmillo, D. P. Baker, R. M. Arduini, K. P. Williams, P. H. Weinreb, P. Rayhorn, X. Hronowski, A. Whitty, E. S. Day, A. Boriack-Sjodin, R. I. Shapiro, A. Galdes, and R. B. Pepinsky. 2001. Enhanced potency of human Sonic Hedgehog by hydrophobic modification. Biochemistry 40:4359–4371.

81. Tempe, D., M. Casas, S. Karaz, M. F. Blanchet-Tournier, and J. P. Concordet. 2006. Multisite protein kinase A and glycogen synthase kinase 3β phosphorylation leads to Gli3 ubiquitination by SCFβTrCP. Mol. Cell. Biol. 26:4316–4326.

82. te Welscher, P., A. Zuniga, S. Kuijper, T. Drenth, H. J. Goedemans, F. Meijlink, and R. Zeller. 2002. Progression of limb development through SHH-mediated counteraction of GLI3. Science 298:827–830.

83. Tian, L., R. A. Holmgren, and A. Matouschek. 2005. A conserved processing mechanism regulates the activity of transcription factors Cubitus interruptus and NF-κB. Nat. Struct. Mol. Biol. 12:1045–1053.

84. Tran, P. V., C. J. Haycraft, T. Y. Besschetnova, A. Turbe-Doan, R. W. Stottmann, B. J. Herron, A. L. Chesebro, H. Qiu, P. J. Scherz, J. V. Shah, B. K. Yoder, and D. R. Beier. 2008. THM1 negatively modulates mouse sonic Hedgehog signal transduction and affects retrograde intraflagellar transport in cilia. Nat. Genet 40:403–410.

85. Varjosalo, M., M. Bjorklund, F. Cheng, H. Syvanen, T. Kivioja, S. Kilpinen, Z. Sun, O. Kallioniemi, H. G. Stunnenberg, W. W. He, P. Ojala, and J. Taipale. 2008. Application of active and kinase-deficient kinome collection for identification of kinases regulating Hedgehog signaling. Cell 133:537–548.

86. Varjosalo, M., and J. Taipale. 2008. Hedgehog: functions and mechanisms. Genes Dev. 22:2454–2472.

87. Wang, B., J. F. Fallon, and P. A. Beachy. 2000. Hedgehog-regulated processing of Gli3 produces an anterior/posterior repressor gradient in the developing vertebrate limb. Cell 100:423–434.

88. Wang, B., and Y. Li. 2006. Evidence for the direct involvement of βTrCP in Gli3 protein processing. Proc. Natl. Acad. Sci. U. S. A. 103:33–38.

89. Wang, C., U. Ruther, and B. Wang. 2007. The Shh-independent activator function of the full-length Gli3 protein and its role in vertebrate limb digit patterning. Dev. Biol. 305:460–469.

90. Wang, G., B. Wang, and J. Jiang. 1999. Protein kinase A antagonizes Hedgehog signaling by regulating both the activator and repressor forms of Cubitus interruptus. Genes Dev. 13:2828–2837.

91. Wang, Y., Z. Zhou, C. T. Walsh, and A. P. McMahon. 2009. Selective translocation of intracellular Smoothened to the primary cilium in response to Hedgehog pathway modulation. Proc. Natl. Acad. Sci. U. S. A. 106:2623–2628.

92. Wigley, W. C., R. P. Fabunmi, M. G. Lee, C. R. Marino, S. Muallem, G. N. DeMartino, and P. J. Thomas. 1999. Dynamic association of proteasomal machinery with the centrosome. J. Cell Biol. 145:481–490.

93. Wilson, C. W., M. H. Chen, and P. T. Chuang. 2009. Smoothened adopts multiple active and inactive conformations capable of trafficking to the primary cilium. PLoS One 4:e5182.

94. Wong, S. Y., and J. F. Reiter. 2008. The primary cilium at the crossroads of mammalian Hedgehog signaling. Curr. Top. Dev. Biol. 85:225–260.

95. Wu, J. T., H. C. Lin, Y. C. Hu, and C. T. Chien. 2005. Neddylation and deneddylation regulate Cul1 and Cul3 protein accumulation. Nat. Cell Biol. 7:1014–1020.

96. Yauch, R. L., S. E. Gould, S. J. Scales, T. Tang, H. Tian, C. P. Ahn, D. Marshall, L. Fu, T. Januario, D. Kallop, M. Nannini-Pepe, K. Kotkow, J. C. Marsters, L. L. Rubin, and F. J. de Sauvage. 2008. A paracrine requirement for Hedgehog signalling in cancer. Nature 455:406–410.

97. Zhang, Q., L. Zhang, B. Wang, C. Y. Ou, C. T. Chien, and J. Jiang. 2006. A Hedgehog-induced BTB protein modulates Hedgehog signaling by degrading Ci/Gli transcription factor. Dev. Cell 10:719–729.